




RESEARCH ARTICLE | JULY 19 2023

A device for studying fluid-induced cracks under mixed-mode loading conditions using x-ray tomography **FREE**

Angel Santarossa ; Laureano Ortellado ; Achim Sack ; Leopoldo R. Gómez ✉; Thorsten Pöschel 



Rev Sci Instrum 94, 073902 (2023)

<https://doi.org/10.1063/5.0145709>



View
Online



Export
Citation

CrossMark

A device for studying fluid-induced cracks under mixed-mode loading conditions using x-ray tomography

Cite as: Rev. Sci. Instrum. 94, 073902 (2023); doi: 10.1063/5.0145709

Submitted: 7 February 2023 • Accepted: 5 July 2023 •

Published Online: 19 July 2023



View Online



Export Citation



CrossMark

Angel Santarossa,¹  Laureano Ortellado,²  Achim Sack,¹  Leopoldo R. Gómez,^{2,a)} 
and Thorsten Pöschel^{1,b)} 

AFFILIATIONS

¹Institute for Multiscale Simulations, Friedrich-Alexander-Universität Erlangen-Nürnberg, Cauerstraße 3, 91058 Erlangen, Germany

²Department of Physics, Universidad Nacional del Sur-IFISUR-CONICET, Av. Alem 1253, Bahía Blanca, Argentina

^{a)} Author to whom correspondence should be addressed: lgomez@uns.edu.ar

^{b)} Electronic mail: thorsten.poeschel@fau.de

ABSTRACT

We introduce an innovative instrument designed to investigate fluid-induced fractures under mixed loading conditions, including uniaxial tension and shear stress, in gels and similar soft materials. Equipped with sensors for measuring force, torque, and fluid pressure, the device is tailored for compatibility with x-ray tomography scanners, enabling non-invasive 3D analysis of crack geometries. To showcase its capabilities, we conducted a study examining crack-front segmentation in a hydrogel subjected to air pressure and a combination of tension and shear stress.

Published under an exclusive license by AIP Publishing. <https://doi.org/10.1063/5.0145709>

I. INTRODUCTION

Hydraulic fracturing, commonly known as fracking, is a prevalent method for stimulating hydrocarbon production by creating a network of fractures around a wellbore.^{1,2} This process involves injecting high-pressure fluid into the rock, resulting in a network of fractures that enhance the reservoir's permeability and increase the surface area for hydrocarbon production. However, current techniques can only recover a small percentage of the estimated hydrocarbons within the rock.^{1,2}

Although enhanced oil recovery is a primary application of hydraulic fracturing, it is also employed in various other contexts. For instance, fracking is used in carbon sequestration, where carbon dioxide is injected into underground rock formations to mitigate greenhouse gas emissions.³ Moreover, natural occurrences of hydraulic fracturing can arise from magmatic intrusions⁴ and water-driven vertical crevassing in glaciers.^{5,6} To optimize production and maintain environmental sustainability,⁷ a comprehensive understanding of the physical mechanisms governing fracture and extraction is essential.

The process of hydraulic fracturing is complex and depends on the solid's anisotropy and the fluid injection's rheology.⁸ Reliable physical models are essential to understand the geometry of fractures. Although hydraulic fracturing has been extensively studied theoretically and numerically,^{9,10} there is comparatively less experimental work on the subject. Only a small number of experiments on the detailed fracture geometry of hydraulic fractures have been reported. In the late 1950s, Hubbert and Willis conducted early qualitative laboratory experiments.¹¹ Subsequently, various groups carried out shape measurements of penny-shaped crack tips.^{12–15} More recently, the dynamics of the formation and evolution of hydraulic fractures in hydrogels have been studied, revealing the formation of step lines due to the interaction between the fragmentation front and material heterogeneity.¹⁶

In general, any type of fracture can be decomposed into three linearly independent modes (Fig. 1).¹⁷ Mode I is the opening mode, which is caused by injecting the fluid and is always the driving mode of hydraulic fracture. Modes II and III are shear modes, which have different effects on fractures. Mode II results in a deviation of the fracture path, while mode III leads to the breaking or segmentation

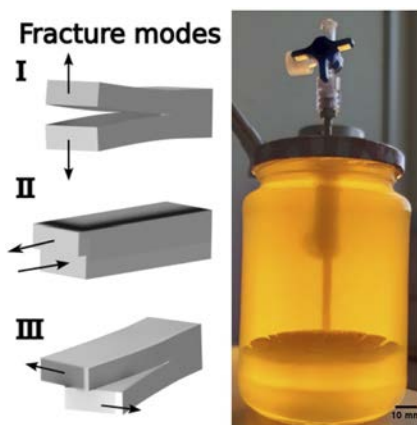


FIG. 1. Fracture modes. Left: Any fracture can be decomposed into three independent modes, an opening mode (I) and two shearing modes (II and III). Right: Hydraulic fracture of hydrogel under combined load modes. Here, the presence of shearing due to the container produces the deviation (II) and segmentation (III) of the fracture front.

of the fracture edges (also known as echelon patterns in geology). While the coupling of modes I and II has been extensively studied both theoretically and experimentally, the effect of mode III is still not well understood.^{18–21} Figure 1 illustrates the presence of all three modes in the hydraulic fracture of a gel. Here, the initial penny-shaped fracture (mode I) evolves a complex shape due to shear modes caused by the boundaries of the container (modes II and III).

An accurate representation of the fracture pattern is essential to understanding the mechanics of hydraulic fracture under specific loading conditions. Transparent materials are usually used to facilitate the observation of fracture geometry and dynamics,^{12–16,19,22–25}

but this restricts the scope of study to certain systems. Furthermore, most studies are limited to 2D observations, which do not fully capture the 3D nature of crack geometry.

In this work, we present a device for studying fluid-drive fractures in 3D using x-ray Computed Tomography (CT). The device is lightweight and designed to be used in an x-ray tomograph and can visualize complex crack morphology. It is made of 3D-printed components, making it affordable and adaptable. The device also includes tension and torque sensors for measuring sample properties during the fracture experiment, as well as a pressure sensor for the fracturing fluid. We demonstrate the device’s functionality by conducting non-invasive experiments on mixed mode I+III air-driven fractures in hydrogels using x-ray CT.

II. INSTRUMENT DESIGN

The setup in Fig. 2 is a measurement module for testing hydraulic fractures under mixed loading conditions. The fracturing sample is obtained through a mold. It is adhered to top and bottom holders for positioning in the experimental module to apply loading conditions [Fig. 2(a)]. The holders have mushroom-shaped components to prevent sample detachment. When subjected to torsional angles higher than 80°, fracture or delamination at these components might occur. To mitigate this issue, the components closer to the gel’s exterior are file to remove any sharp edges that may result from the 3D printing process. The bottom holder is fixed while the top holder can be displaced and rotated to impose uniaxial and shear strain [Fig. 2(b)]. The top holder also allows for placing a fluid injection needle at a desired depth. Various fluid can be used for testing as long as they provide enough contrast in x-ray imaging.

The measurement module is a lightweight structure crafted from plastic (polyamide 12) using 3D printing techniques, rendering it compatible with x-ray tomography. The corresponding STL file can be obtained in the supplementary material. The choice of

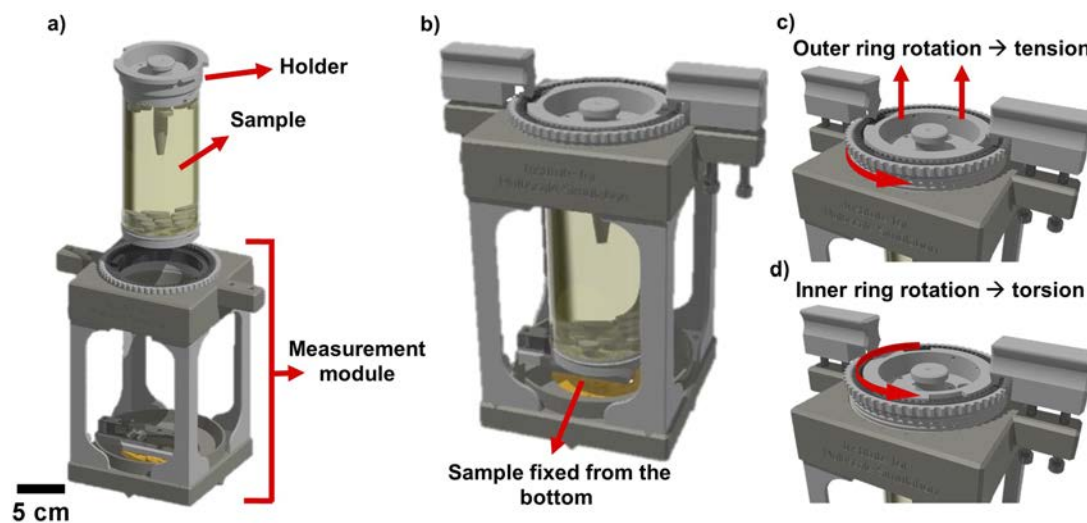


FIG. 2. Experimental setup. The sample is mounted to the measurement module (a) and is fixed at the base (b). Two modes of loading can be applied: tension (c), by elongating the sample through the rotation of an outer ring, and shear stress (d), by rotating an inner ring that induces torsion.

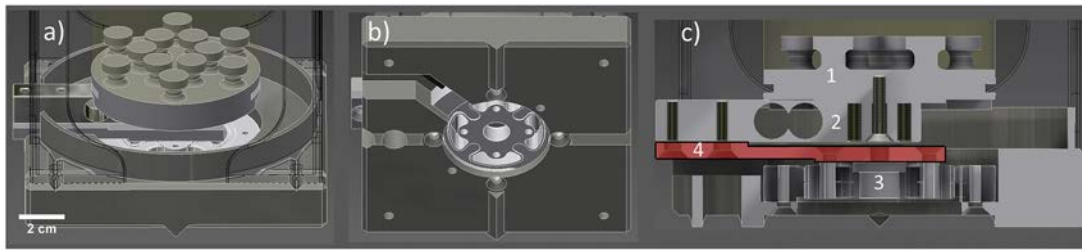


FIG. 3. Sensors. (a) and (b) Force and torque sensors are located at the base of the measurement module. (c) The bottom holder of the sample (1) is attached to the cantilever force sensor, while the force sensor is simultaneously connected to the torque sensor (3) through an aluminum part [(4), highlighted in red]. This setup enables the simultaneous measurement of both force and torque because it allows for deflection of the beam.

plastic material is based on its low x-ray absorption characteristics and its resilience compared to hydrogels, making it a suitable device for soft materials fracture testing. The module has two rings on the top, which are used to apply different types of loads on the sample [Fig. 2(c)]. The outer ring can be screwed to adjust the sample's height and apply uniaxial tension. A displacement sensor is used to measure the elongation of the sample and prescribe an initial strain value. The inner ring allows for the rotation of the sample to a specific angle and, in turn, the application of torque. The inner ring is mounted in a ball bearing to reduce friction and ensure smooth rotation. Two mechanical clamps, one at each side of the setup, fix the position of the inner ring and, therefore, the value of the specimen's torsion angle.

The measurement module is equipped with a force sensor (DIYmalls 5 kg load cell) and a torque sensor (TS70a-10Nm, ME-Systeme) at its base to record the tension and torsion applied to the sample during a fracture experiment [see Figs. 3(a) and 3(b)]. Figure 3(c) shows that the bottom of the sample (1) is fixed on the force (2) and torque (3) sensors. To that aim, the sample is first attached to the end of a cantilever force sensor and then fixed to the torque sensor through an aluminum holder, allowing for the measurement of the cantilever's deflection (4). Additionally, the pressure of the injected fluid is recorded by a sensor connected to a hose linked to the needle.

To pump the fracturing fluid we use an in-house designed injection system. A plastic syringe of diameter $d = 2$ cm and of maximum volume $V_{\max} = 20$ ml is fixed to the pump. The injection system consists of a screw, whose rotation displaces the piston of the syringe, thus forcing the contained fluid to flow. The fluid's flow rate can be set to an approximately constant value (in the range of 0.005–3 ml/s).

III. SAMPLE APPLICATION

To demonstrate the apparatus, we study the segmentation of crack fronts in brittle gelatin-based hydrogels during mixed mode I–III air-driven fractures. Hydrogels serve as model systems for the investigation of various types of fractures^{23,24} and have been used to analyze the coalescence of coplanar penny-shaped fractures,²⁶ the progression of viscous and toughness-dominated cracks,¹³ and the dynamics of foam-driven fractures.¹⁴ The experiment involves inducing mixed mode I+III through mechanical stress during hydraulic fracture and using x-ray CT imaging to create a 3D representation of the crack geometry.

A. Sample preparation

Cylindrical samples, measuring 4.3 cm in diameter and 13.5 cm in height, are produced through a molding process. The gel for the

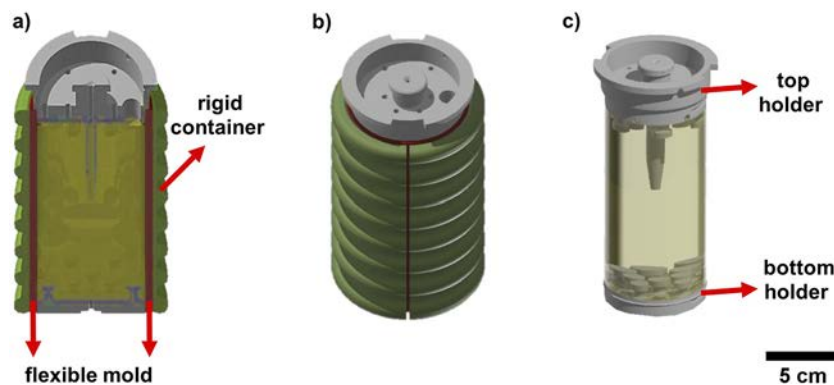


FIG. 4. Molding process: (a) Cross-sectional view of the mold filled with liquid gel. A flexible vessel, housed within a rigid container, is employed to maintain the sample's cylindrical shape during solidification. (b) Assembled mold for sample preparation. The molten gel is introduced through the openings at the top of the mold. (c) Sample post-demolding. The gel's exterior surface remains unconfined (free surface).

samples is created by dissolving 100 g of commercial gelatin in a mixture of 0.5 l of distilled water and 0.5 l of glycerin. The solution is heated to 55° and stirred until the gelatin is completely dissolved. It is then poured into a mold and cured at a temperature of 5° for roughly 24 h before being removed from the mold. The gelatin is dissolved in a glycerol–water solvent to improve its elasticity.²⁷ Low-frequency rheology at 7 °C shows that the shear modulus is $\sim 10^4$ Pa in good agreement with a reported study in similar conditions.²⁸ Similar gelatin-based gels have reported fracture toughness values $\lesssim 10$ N/m.²⁹ Typically, commercial hydrogels have a limited shear modulus, usually not exceeding 10^5 Pa, for which this setup is capable of performing fracture experiments.^{30,31}

The mold used in this process consists of four parts, as shown in Figs. 4(a) and 4(b). The top and bottom holders, which remain adhered to the sample after curing, are located in a flexible cylindrical container made of resin using a Formlabs Form 3+3D printer. The container is coated with silicone to prevent adhesion of the gelatin during the curing process. The flexible mold is then placed within a rigid container to maintain the cylindrical shape of the fracturing sample after demolding. Upon the gel's solidification both the flexible and rigid containers are detached, as illustrated in Fig. 4(c). Following the demolding procedure, the exterior of the gel emerges as an unconstrained surface. To prevent fracturing of the elastic matrix during injection, a 2 mm diameter needle is located in the top holder before the curing of the gel. To prevent blockage of the fracturing fluid a thread is placed within the needle before curing, which impedes the flow of the liquid gel inside the needle due to capillary forces.

B. Hydraulic fracture in mixed mode I+III

In a typical hydraulic fracture experiment, the following steps are carried out:

1. The gel sample is mounted on the measurement module and securely attached to the force sensor.
2. The thread inside the needle is removed.
3. Strain is applied to the sample (mode I) by adjusting the height of the sample using the outer ring of the measurement module until a small penny-shaped pre-fracture is formed next to the needle. The size and orientation of this crack are relatively uniform across experiments, typically appearing horizontal and about 1 cm in diameter.
4. The penny-shaped fracture is enlarged by injecting 2 ml of air at a slow rate (0.01 ml/s) to avoid sudden pressure changes.
5. Torsion (mode III) is applied to the sample by adjusting manually the inner ring of the measurement module to a desired angle.
6. Additional air is injected through the needle, creating a hydraulic fracture under mixed conditions and resulting in the segmentation of the fracture front.
7. Once the fracture reaches the boundaries of the sample, the injection of air is halted and the fluid connection is closed with a valve to prevent backflow and the closure of the fracture.

During a hydraulic fracture experiment, both force and torque acting on the sample, as well as the pressure of the fracturing fluid are recorded. To maintain a constant temperature, the experiment is

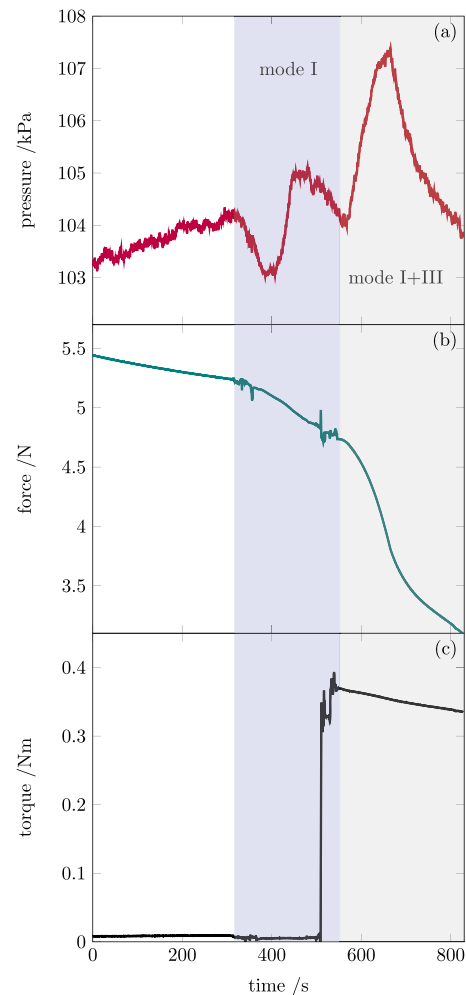


FIG. 5. Tension (b) and torque (c) on the sample and fluid pressure (a), in time, throughout a fracture experiment. The data shown correspond to a mixed mode I + III fracture performed with air for 6 mm of gel's elongation and 50° of torsion angle. The gray shaded area represents a mixed mode I + III fracture, while the blue shaded is a pure mode I.

performed in a refrigerator. Figure 5 illustrates the typical time evolution of tension, torque, and fluid pressure during the experiment, which shows the formation and propagation of cracks. Initially, fluid pressure escalates, reaching its peak at the moment of gel fracture. As the fracture propagates, both fluid pressure and sample tension diminish. Upon applying torsion to the sample, it experiences mixed mode I+III loading. The crack, as it progresses under these mixed loading conditions, becomes fragmented, exhibiting inclined facets. This fragmentation increases the crack's surface area, necessitating higher pressure for further advancement, as illustrated in Fig. 5(a).

It is noteworthy that examining the time evolution of pressure, force, and torsion during fracture can be instrumental in understanding the behavior of materials with complex dynamic responses, as well as the behavior of fracturants exhibiting complex characteristics.³²

TABLE I. Parameters used for x-ray CT.

Parameter	Value
Source voltage	140 kV
Target current	270 μ A
Projections per scan	800
Measurements per projection	5
Exposure time	100 ms
Resolution	85.44 μ m ⁻¹

It is noteworthy that examining the time evolution of pressure, force, and torsion during fracture can be instrumental in understanding the mechanics of fractures driven by fluid exhibiting complex rheological properties, such as non-newtonian behavior.³² For instance, most fluid used in hydraulic fracturing for oil and gas stimulation show shear thinning behavior.³³ Furthermore, compressible aqueous-foam fluid are used as a sustainable alternative in conventional hydraulic fracturing to reduce the usage of water.^{34,35} In both cases, it has been shown that rheological features of the fluid strongly influence the formation and propagation of fluid-induced cracks.^{14,33}

The final fracture geometry produced under mixed loading conditions is complex, and precise measurement of the facets' angle can be obtained using tomography. Therefore, following hydraulic fracturing, we employ x-ray tomography to visualize the fragmentation pattern. The tomographic images are acquired using a lab tomograph, and the Xray-Office software (v2.0) is used to generate a 3D representation of the crack. The acquisition parameters are provided in Table I. Image processing and segmentation are performed with itk-SNAP.³⁶ In addition to reconstructing a 3D image through post-mortem x-ray analysis, the device can also be utilized for *in situ* measurements. In this approach, the sample is scanned sequentially after injecting small amounts of fluid enabling the examination of fracture growth at consecutive stages.

The top panel of Fig. 6 displays a 3D reconstruction of a crack in a gelatin hydrogel. In this experiment, the sample was initially subjected to uni-axial tension by displacing the top holder by 8 mm (6%), leading to a penny-shaped prefracture (mode I). Subsequently, torque was applied by rotating the top holder by 50°, resulting in a segmented fracture with tilted facets. The inclination of the facets originates due to piecewise adjustment of the crack front plane to changes in the directions of the maximum principal stress at the crack tip in a plane perpendicular to the direction of crack propagation.^{25,37} It is noteworthy that the tilted facets (also referred to as type A cracks) are not connected by slanted cracks (known as type B cracks) but instead by a region that remains uncracked or breaks later, as observed in other studies.^{22,25} The formation of type B cracks is energetically unfavorable due to their unfavorable orientation concerning the local opening mode I.^{22,38}

In this study, we also conducted fracture experiments with a different balance of modes I and III. The central panel of Fig. 6 presents the 3D reconstruction of a crack created using the same method as previously mentioned but with the top holder rotated by 30°. Generally, the number of facets and the tilt angle depend on the balance between modes I and III during fracture,³⁷ with the

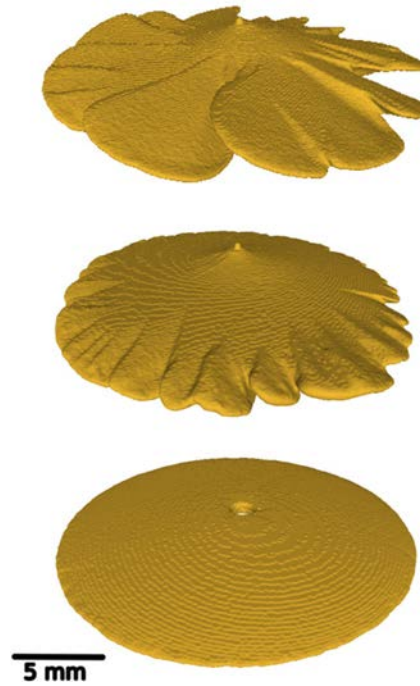


FIG. 6. The visualization of crack geometries in mixed modes I+III fractures was carried out using air, with an 8 mm elongation of the gel. The top panel features a 3D reconstruction of the crack achieved at a 50° torsion angle. The mean tilt angle of the leaves relative to the parent planar crack is $13^\circ \pm 2^\circ$, and the number of fully fragmented facets is 11. The middle panel illustrates the crack geometry obtained at a 30° torsion angle. In this case, the number of fully segmented leaves is 25, and the average tilt angle of the facets is $7^\circ \pm 2^\circ$. Finally, the bottom panel displays a penny-shaped unsegmented fracture resulting from zero torsion (a mode I driven fracture). The small-scale roughness observed in the 3D renderings of the cracks can be primarily attributed to digitization artifacts after image processing.

facets' inclination angle increasing with the angle of the shear deformation of the gel. As anticipated, the tilt angle of the facets is smaller in this case. Additionally, there are more facets or petals with this loading condition. Finally, the bottom panel of Fig. 6 illustrates the fracture obtained without rotation of the top holder (no torsion). In this situation, the fracture assumes the typical penny-shaped form, commonly observed during hydraulic fracture when only mode I is present.

IV. SUMMARY

We introduced a new experimental apparatus for investigating fluid-induced fractures under combined uniaxial tension and shear stress. The device, designed for x-ray tomography scanning, enables non-invasive 3D analysis of complex fracture morphologies, which are often challenging to observe and analyze using traditional methods. It includes sensors for measuring tension, torque, and fluid pressure. Its 3D-printed components are cost-efficient and easy to modify. By demonstrating its functionality through an example of crack-front segmentation in a mixed-mode I+III air-driven fracture in a hydrogel, we have highlighted the device's capability in applying different loading conditions purely mechanically. The apparatus can

also be used to study fractures in other types of gels and soft materials,³² such as silicones, using various fracturing fluids⁸ making it a valuable tool for researchers in various fields

This work has presented an example of hydraulic fracturing under mixed loading conditions in a toughness-dominated regime,³⁹ where the fracture process is predominantly governed by the material's fracture toughness. Nevertheless, this experimental setup can be adapted to study fractures in other regimes, including viscous fluid-dominated regimes and more. The device's ability to offer detailed, three-dimensional insights into fracture morphology paves the way for new possibilities in understanding and controlling fluid-induced fractures.

SUPPLEMENTARY MATERIAL

As a supplementary material to this study, we have included the STL file necessary for 3D printing the measurement module used to test hydraulic fractures under mixed loading conditions.

ACKNOWLEDGMENTS

A.S. and T.P. gratefully acknowledge funding by the Deutsche Forschungsgemeinschaft (DFG) through the Research Training Group GRK 2423 "Fracture across Scales-FRASCAL" (Grant No. 377472739/GRK2423/1-2019). This work was supported by the BAYLAT (Germany)-CONICET (Argentina) cooperation initiative, the Interdisciplinary Center for Nanostructured Films (IZNF), the Competence Unit for Scientific Computing (CSC), and the Interdisciplinary Center for Functional Particle Systems (FPS) at Friedrich-Alexander University Erlangen-Nürnberg. This work was also supported by the National Research Council of Argentina, CONICET (Grant No. PIP 11220200103059), the Fondo para la Investigación Científica y Tecnológica (FONCYT, Grant Nos. PICT-2017-3611 and PICT-2021-1272), and Universidad Nacional del Sur. L.R.G. acknowledges support from the Humboldt foundation through the Georg Forster and return fellowships. L.O. expresses gratitude for the support provided by DAAD through their Research Grants—Short-Term Grants program in 2022.

AUTHOR DECLARATIONS

Conflict of Interest

The authors have no conflict to disclose.

Author Contributions

Angel Santarossa: Conceptualization (supporting); Data curation (equal); Investigation (equal); Methodology (equal); Software (equal); Visualization (equal); Writing – original draft (equal); Writing – review & editing (supporting). **Laureano Ortellado:** Conceptualization (supporting); Data curation (equal); Investigation (equal); Methodology (equal); Software (equal); Visualization (equal); Writing – original draft (supporting); Writing – review & editing (equal). **Achim Sack:** Conceptualization (supporting); Data curation (supporting); Investigation (supporting); Methodology (supporting); Resources (supporting). **Leopoldo R. Gómez:** Conceptualization (lead); Data curation (supporting); Formal analysis

(supporting); Funding acquisition (lead); Investigation (lead); Methodology (lead); Project administration (lead); Supervision (lead); Writing – original draft (equal); Writing – review & editing (equal). **Thorsten Pöschel:** Conceptualization (lead); Funding acquisition (lead); Investigation (lead); Methodology (lead); Project administration (lead); Resources (lead); Writing – original draft (lead); Writing – review & editing (lead).

DATA AVAILABILITY

The data that support the findings of this study are available from the corresponding author upon reasonable request.

REFERENCES

- 1 P. Valkó and M. J. Economides, *Hydraulic Fracture Mechanics*, vol.28 (Wiley, Chichester, 1995).
- 2 D. L. Turcotte, E. M. Moores, and J. B. Rundle, *Phys. Today* **67**(8), 34 (2014).
- 3 P. Fu, R. R. Settigast, Y. Hao, J. P. Morris, and F. J. Ryerson, *J. Geophys. Res.: Solid Earth* **122**, 9931, <https://doi.org/10.1002/2017jb014942> (2017).
- 4 A. M. Rubin, *Annu. Rev. Earth Planet. Sci.* **23**, 287 (1995).
- 5 R. B. Alley, T. K. Dupont, B. R. Parizek, and S. Anandakrishnan, *Ann. Glaciol.* **40**, 8 (2005).
- 6 C. J. van der Veen, *Geophys. Res. Lett.* **34**, L01501, <https://doi.org/10.1029/2006gl028385> (2007).
- 7 A. Vengosh, R. B. Jackson, N. Warner, T. H. Darrah, and A. Kondash, *Environ. Sci. Technol.* **48**, 8334 (2014).
- 8 A. C. Barbati, J. Desroches, A. Robisson, and G. H. McKinley, *Annu. Rev. Chem. Biomol. Eng.* **7**, 415 (2016).
- 9 E. Detournay, *Annu. Rev. Fluid Mech.* **48**, 311 (2016).
- 10 J. Adachi, E. Siebrits, A. Peirce, and J. Desroches, *Int. J. Rock Mech. Min. Sci.* **44**, 739 (2007).
- 11 M. K. Hubbert and D. G. Willis, *Trans. AIME* **210**, 153 (1957).
- 12 A. P. Bungler, *Meas. Sci. Technol.* **17**, 3237 (2006).
- 13 C.-Y. Lai, Z. Zheng, E. Dressaire, J. S. Wexler, and H. A. Stone, *Proc. R. Soc. A* **471**, 20150255 (2015).
- 14 C.-Y. Lai, B. Rallabandi, A. Perazzo, Z. Zheng, S. E. Smiddy, and H. A. Stone, *Proc. Natl. Acad. Sci. U. S. A.* **115**, 8082 (2018).
- 15 N. J. O'Keefe, H. E. Huppert, and P. F. Linden, *J. Fluid Mech.* **844**, 435 (2018).
- 16 W. Steinhardt and S. M. Rubinstein, *Phys. Rev. Lett.* **129**, 128001 (2022).
- 17 J. R. Rice *et al.*, "Mathematical analysis in the mechanics of fracture" in *Fracture: an Advanced Treatise*, edited by H. Liebowitz (Academic Press, NY, 1968), 2, pp. 191–311.
- 18 D. D. Pollard, P. Segall, and P. T. Delaney, *Geol. Soc. Am. Bull.* **93**, 1291 (1982).
- 19 R. Wu, L. N. Germanovich, P. E. Van Dyke, and R. P. Lowell, *J. Geophys. Res.: Solid Earth* **112**, B05209, <https://doi.org/10.1029/2005jb003815> (2007).
- 20 A. J. Pons and A. Karma, *Nature* **464**, 85 (2010).
- 21 C.-H. Chen, T. Cambonie, V. Lazarus, M. Nicoli, A. J. Pons, and A. Karma, *Phys. Rev. Lett.* **115**, 265503 (2015).
- 22 K. H. Pham and K. Ravi-Chandar, *Int. J. Fract.* **199**, 105 (2016).
- 23 N. J. O'Keefe and P. F. Linden, *Exp. Mech.* **57**, 1483 (2017).
- 24 Z. Li, J. Wang, and I. D. Gates, *Rock Mech. Rock Eng.* **53**, 4345 (2020).
- 25 E. Sommer, *Eng. Fract. Mech.* **1**, 539 (1969).
- 26 N. J. O'Keefe, Z. Zheng, H. E. Huppert, and P. F. Linden, *Proc. Natl. Acad. Sci. U. S. A.* **115**, 10228 (2018).
- 27 S. Sanwlani, P. Kumar, and H. B. Bohidar, *J. Phys. Chem. B* **115**, 7332 (2011).
- 28 J. van Otterloo and A. R. Cruden, *Tectonophysics* **683**, 86 (2016).
- 29 M. Czerner, L. A. Fasce, J. F. Martucci, R. Ruseckaite, and P. M. Frontini, *Food Hydrocolloids* **60**, 299 (2016).
- 30 R. Ferraro, S. Guido, S. Caserta, and M. Tassieri, *Soft Matter* **19**, 2053 (2023).

- ³¹E. Di Giuseppe, F. Funicello, F. Corbi, G. Ranalli, and G. Mojoli, *Tectonophysics* **473**, 391 (2009).
- ³²D. Ozturk, M. L. Morgan, and B. Sandnes, *Commun. Phys.* **3**, 119 (2020).
- ³³F.-E. Moukhtari and B. Lecampion, *J. Fluid Mech.* **838**, 573 (2018).
- ³⁴D. Mack and L. Harrington, *Oil Gas J.* **88**, 49–58 (1990).
- ³⁵R. S. Bullen and T. F. Bratrud, *J. Can. Pet. Technol.* **15**, 27–32 (1976).
- ³⁶P. A. Yushkevich, J. Piven, H. C. Hazlett, R. G. Smith, S. Ho, J. C. Gee, and G. Gerig, *Neuroimage* **31**, 1116 (2006).
- ³⁷M. L. Cooke and D. D. Pollard, *J. Geophys. Res.* **101**, 3387, <https://doi.org/10.1115/95jb02507> (1996).
- ³⁸V. Lazarus, J.-B. Leblond, and S.-E. Mouchrif, *J. Mech. Phys. Solids* **49**, 1421 (2001).
- ³⁹D. Garagash and E. Detournay, *J. Appl. Mech.* **67**, 183(2000).